Depletion-induced fractionation of optically anisotropic particles

2002 J. Phys.: Condens. Matter 14 7563

(http://iopscience.iop.org/0953-8984/14/33/302)

INSTITUTE OF PHYSICS PUBLISHING JOURNAL OF PHYSICS: CONDENSED MATTER

J. Phys.: Condens. Matter **14** (2002) 7563–7580 PII: S0953-8984(02)38471-6

Depletion-induced fractionation of optically anisotropic particles

R Piazza[1], **S Iacopini, M Pierno and E Vignati**

INFM, Dipartimento di Ingegneria Nucleare, Politecnico di Milano, via Ponzio 34/3, 20133 Milano, Italy

E-mail: roberto.piazza@polimi.it

Received 21 June 2002
Published 9 August 2002
Online at stacks.iop.org/JPhysCM/14/7563

Abstract

We show that depletion forces induced by surfactant micelles can be profitably exploited to perform an efficient *a posteriori* size fractionation of suspensions of optically anisotropic colloids. Efficiency and limits of the fractionation protocol are discussed both on 'model' and technical polydisperse lattices. This method can be used to single out fractions composed by long fibrillar particles, showing evidence of mesogenic behaviour. Depolarized dynamic light scattering is used to extract the particle translational and rotational diffusion coefficients D_T and D_R as a function of particle volume fraction. Both the concentration behaviour of D_T and the full shape of the depolarized correlation functions show distinctive and partially unexpected features.

1. Introduction

Since this is, after all, a special issue in honour of Peter Pusey, let us start with a personal memory. Some years ago (it must have been around 1991), the first author of this paper was travelling back from a meeting together with Peter. Those years had been extremely fruitful for colloid physics studies, so much that the author was wondering if there was still something relevant left to do with 'model' particles, or whether it was better to start playing with different things. The latter was not Peter's point of view. With one of his usual understatements, he said that he was 'mixing colloids with polymers', and observing things that 'could have been of some interest'. I was not particularly excited by the topic, and just said to myself 'this is still the same old story about physicists, deliberately making things messy in order to *build* new problems—look how different is for biologists, who don't need at all to *look* for problems!'. This omen surely does not match more illustrious ones about the impossibility of building atomic weapons, or selling more than a few hundreds PCs, but still points out how poorly a physicist can play Cassandra. In a few years, indeed, the understanding of depletion forces

[1] Author to whom any correspondence should be addressed.

stemming from Peter's joint work with other first-class scientists [1] has shed totally new light on a whole class of phenomena, including many related to biology [2], and opened up interesting theoretical questions about the phase behaviour [3] and metastability [4] of systems interacting via a short-range potential.

Although dealing with the same topic, this paper faces more mundane and practical issues. Namely, can we *exploit* depletion forces in order to obtain colloidal systems of interest that cannot be directly synthesized? Obtaining monodisperse particles is of primary importance for basic colloid physics studies but, although ingenious methods have been found to produce monodisperse spheres, most synthesis methods of inorganic and polymer colloids yield particle-size distributions which are at best relatively narrow. This is particularly true when particle synthesis involves delicate and sometimes dangerous chemical steps, which can hardly be performed in a research laboratory, and force the investigator to be content with samples made in large plants. Fluorinated latex particles, which show very peculiar and interesting features, unluckily belong to this category. In this paper we show however that surfactant-induced depletion forces can be profitably exploited for an efficient *a posteriori* particle size fractionation of polydisperse fluorinated lattices.

Surfactant-induced fractionation has been demonstrated by Bibette in his pioneering work on SDS emulsions, and used to obtain very monodisperse oil droplets [5]. Size-dependent phase segregation is in this case introduced by excess of the very same ionic surfactant which stabilizes the oil droplets, and which is supposed to act as a depleting agent when dispersed in the continuous phase in micellar form. Later, Piazza and Di Pietro [6] showed that similar effects can be obtained by adding a few per cent nonionic surfactant to a polymer colloid latex, and that the phase behaviour of the system is consistent with what is expected for particles interacting via very strong short-range depletion forces induced by the surfactant micelles. While in the emulsion case both the original droplet size distribution and the depletion effects are determined by surfactant concentration, this latter method allows us to control separately the nature of the dispersion to be fractionated and the depletion effects, therefore allowing for a detailed study of the fractionation efficiency. An additional advantage of nonionic-surfactant fractionation is that it can be finely tuned by temperature, since micellar-induced depletion effects show a large enhancement near the lower consolution curve of these agents with water, with universal features depending only on the temperature distance from the critical point [7]. It is important to notice that two distinct phenomena take place by progressively adding the nonionic surfactant, which first adsorbs on the particle surface, forming a sterically stabilizing layer, and then, when full surface coverage is reached, forms micelles which act as depleting agent. The first crucial step requires a *hydrophobic* particle surface. For *hydrophilic* surfaces such as silica, surfactant micelles (which probably adhere to the particle surface) very often act as a coagulating agent.

In this paper, the previous findings are first exploited in order to single out some additional features of surfactant-induced fractionation, and to inquire about its efficiency. We shall consider three exemplifying situations.

(i) By preparing a controlled bimodal distribution of spherical particles, we show that particles of larger size can be singled out, severely reducing the concentration of the smaller component.

(ii) By repeated separation of fairly polydisperse lattices, we show that fairly monodisperse fractions of rodlike particles can be obtained.

(iii) Finally, we show that this method can be used to 'slice down' very narrow size distributions, and filter out particle fractions that are too small to be detected even by using sensitive methods such as dynamic light scattering (DLS).

In the second part, we present an exploratory survey of a system of very long rodlike fluorinated particles obtained by large-batch fractionation and a preliminary study of the particle translational and rotational diffusion coefficients approaching a nematic phase.

2. Materials and methods

All measurements have been performed on suspensions of fluorinated polymer colloids, kindly supplied by Ausimont S.p.A., Milano (Italy). Such particles, made of polytetrafluoroethylene (PTFE) or tetrafluoroethylene copolymers with perfluoroalkylvinylethers (PFA) or hexafluoropropene (FEP), have very distinctive optical properties [8]. First of all, their average refractive index is very similar to that of water, allowing optical studies of concentrated suspensions. Moreover, they are optically anisotropic due to their partial crystallinity, and therefore scatter a noticeable amount of depolarized light. In addition to this, since the density of PTFE is quite high ($\rho \approx 2.2$), phase separation processes take place in a relatively short timescale (of the order of tens of minutes). The properties of the specific batches which have been used are stated within the description of each single experiment. As a depleting agent, we have used the nonionic surfactant Triton X100 (Room & Haas). The general sample preparation protocol is the following. A dilute particle batch is sterically stabilized by adding an amount of Triton sufficient for full particle surface coverage. This can be achieved by adding a surfactant volume fraction $\Phi_S \approx (3d/R)\Phi_P$, where $d \approx 2$ nm is the approximate length of the surfactant chain, R the particle radius and Φ_P the particle volume fraction. Once stabilized, the particles do not show coagulation up to ionic strengths in the molar range. In order to screen electrostatic effects, a fairly concentrated NaCl solution is added to reach a final ionic strength $I = 100$ mM l^{-1}. Additional Triton, which goes into solution in micellar form and plays the role of the depleting agent, is then progressively added to the solution. When phase separation is observed, the sample vials are left to equilibrate for one day. The relative volume of the separated phase at the bottom of the cell is approximately evaluated by measuring the height of the sediment, and then the separated phase and the supernatant are sampled. Measurements of the size distribution of the original samples and of the separated phases are made by DLS using a Brookhaven BI 9000 multiple-sample-time correlator. Our scattering apparatus allows us to perform depolarized dynamic light scattering (DDLS) measurements of the particle rotational diffusion coefficient D_R. Since D_R scales as the inverse of the cube of the particle radius, DDLS measurements are much more sensitive to particle polydispersity than 'conventional' DLS. The results collected in figure 1, which refer to measurements performed both on fluorinated and on calibration standard polystyrene lattices (Polyscience, USA), show that the minimum amount of surfactant needed to trigger phase separation scales roughly as the inverse of the particle radius R. This trend can be understood by observing that for small values of the size ratio r/R, where r is the micellar radius, the depletion potential at contact is given by $U/k_BT \approx 3R\Phi_S/(2r)$, with Φ_S denoting the volume fraction of micelles. From this expression, the observed scaling follows directly once it is assumed that phase separation takes place below a fixed critical value of the potential at contact.

3. Features of the depletion–fractionation process

3.1. Model mixtures of spherical colloids

In order to test the effectiveness of the separation method, we have studied mixtures of monodisperse PFA particles having radius $R_1 = 75$ nm and FEP particles with radius

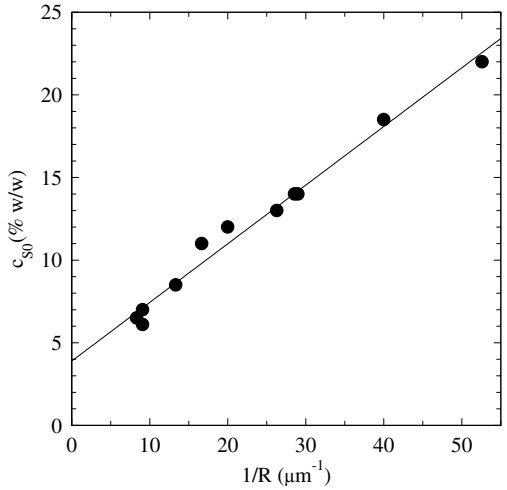

Figure 1. Minimum amount c_{S0} of Triton X100 needed to induce phase separation of colloidal lattices, as a function of the reciprocal particle size. Data refer to both fluorinated and polystyrene monodisperse colloids.

$R_2 = 39$ nm. A 30% w/w Triton solution, prepared in 100 mM l^{-1} NaCl, was progressively added to a mixture specifically prepared at particle volume fraction $\Phi_1 = 0.006$ of PFA particles to a FEP suspension at volume fraction $\Phi_2 = 0.025$ (sample M_0). Clouding followed by phase segregation was first observed for Triton concentration $c_S = 8.5\%$ w/w. The sample was left to equilibrate for a day, and then the lower phase (sample M_1) was extracted. More Triton was then added to the surnatant phase, until a second phase separation was detected for $c_S = 13\%$ w/w. The lower phase was once again extracted (sample M_2). After this second extraction, the supernatant phase scattered very weakly, showing that almost all colloidal particles had separated in the first two steps. The process was nonetheless carried on, but no further signs of clouding or phase separation were observed up to a Triton concentration $c_S = 16\%$ w/w. Notice that the values of c_S marking the onset of the two segregation processes coincides with those needed, according to figure 1, to phase separate pure PFA and FEP.

The dense separated phases were abundantly diluted in water, in order both to suppress multiple scattering and to reduce the overall Triton concentration to values which do not appreciably affect the solvent viscosity. Figure 2 compares the DLS scattered field correlation functions $g_1(t)$ obtained for the initial mixture and for sample M_1 with those measured for pure PFA and FEP suspensions in a Triton/water solution at the same surfactant concentration. While sample M_0 shows a behaviour intermediate between those found for the two pure components, the experimental $g_1(t)$ obtained for sample M_1 is essentially indistinguishable from the correlation function for a pure PFA suspension. The initial decay rate of the original mixture $\Gamma = 1410$ s^{-1} is reasonably consistent with the value $\Gamma = 1370$ s^{-1}, calculated from a molecular weight average of the decay rates of the pure components. The decay rate for sample M_1 instead differs by about 4% from the value obtained for pure PFA. Such a value for the decay rate implies that the concentration ratio of FEP to PFA in sample M_1 is reduced by at least a factor of ten compared with sample M_0. Since the total volume of the first separated phase amounts to about $1/20$ of the original batch volume, most of the residual FEP is probably due to particles 'geometrically trapped' within the separated PFA phase, and could therefore be further reduced starting, for instance, from more dilute suspensions. The

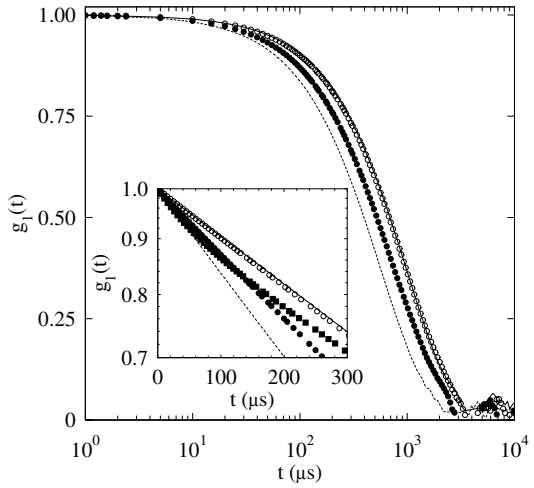

Figure 2. Field correlation functions for the original FEP + PFA mixture M_0 prepared according to the text (●) and for the first separated fraction M_1 (○). Full and dotted curves are correlation functions obtained for pure PFA and FEP respectively. The inset, giving the short-time behaviour of the correlation functions on a linear scale, also highlights the non-exponential shape of the correlation function for fraction M_2 (■).

situation is different for sample M_2, whose correlation function is also shown in the inset. Although the first cumulant of $g_1(t)$ does not differ too much from the value for pure FEP, the correlation function shows a noticeable deviation from the exponential shape even at short time. This may be partly due to the residual presence of PFA particles that partitioned between the two phases during the first separation process. When phase separation occurs at high surfactant concentration as for sample M_2, we also notice however the presence of larger particle aggregates that do not dissolve by dilution. The separation protocol therefore looks very efficient for PFA particles, but poor for FEP.

3.2. Fractionation of polydisperse suspensions

We have applied the depletion–fractionation method to polydisperse lattices of pure PTFE particles obtained by Ausimont using microemulsion (μE) polymerization. In fairly controlled conditions, this synthesis method yields suspensions displaying the co-presence of spherical and rodlike particle morphologies. Moreover, μE polymerization of PTFE yields particles which apparently have a much more pronounced crystallinity compared with conventional emulsion polymerization, and which therefore show much larger optical anisotropy. Transmission electron microscopy pictures of the specific suspension we shall refer to (batch A), which had a total solid content of about 18% w/w, revealed a broad particle size distribution that, although very skewed towards small sizes, showed the distinctive presence of rodlike particles. An index-match curve of the batch gives an average refractive index $\bar{n} \approx 1.37$ and an optical anisotropy $\Delta n \approx 0.08$ (about twice the value found for short PTFE rods obtained by conventional emulsion polymerization), so the scattering in pure water is only about twice that in 'best-matching' conditions.

Aiming to 'tune' the fractionation protocol, we first prepared small samples with fixed particle volume fraction $\Phi \approx 0.05$ and Triton concentration c_S varying from 3 to 12%, in the presence of 100 mM l^{-1} NaCl. Samples with c_S above a threshold value $c_S \approx 6\%$

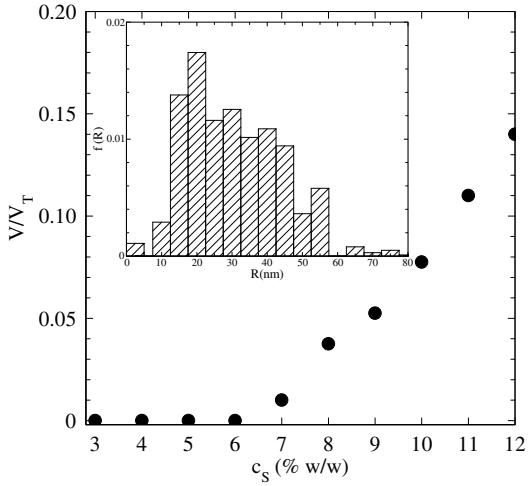

Figure 3. Ratio V/V_T of separated to total volume for batch A as a function of surfactant concentration c_S. The inset shows the approximate particle size distribution for the original sample batch as obtained from DLS measurements.

showed a rapid turbidity enhancement and fully phase-separated in a timescale of a few hours, leaving a thick, strongly scattering sediment at the bottom of the cell. Figure 3 shows that the ratio V/V_T of the separated phase to the total sample volume increases almost linearly with surfactant concentration above the threshold value. A larger sample (about 25 ml) at an initial Triton concentration $c_S = 7\%$ was then prepared and allowed to separate for about one day. We then extracted the lower separated phase (sample A_1, with a volume of about 0.5 ml), and the upper phase was titrated to $c_S = 9\%$, adding a concentrated Triton solution, and allowed to fully separate. The bottom phase was again extracted (sample A_2), and the whole protocol was repeated by increasing the surfactant concentration up to 12%, obtaining sample A_3. In each stage of this fractionation procedure, a small amount of the surnatant phase was also sampled. A further increase of c_S to 15% yielded a very small amount of separated phase. Nonetheless, the surnatant still scattered noticeably, showing that a conspicuous amount of particles had not been separated out from the original suspension.

In order to have a better estimate of their composition, the original suspension (sample A_0) and the fractionated phases have been studied by DDLS, which, as we have said, gives a better resolution than DLS for low degrees of polydispersity. Let us simply recall that, for dilute suspensions of monodisperse spherical particles, the decay rate Γ_{VH} of the field correlation function $g_{VH}(t)$ measured in VH geometry (that is, by detecting the horizontal polarization component of the light scattered from a vertically polarized beam) is given by $\Gamma_{VH} = D_T q^2 + 6D_R$, where D_T and D_R are the particle translational and rotational diffusion coefficients and q is the scattering wavevector. Normally, depolarized scattering is so weak that the solvent composition has to be modified in order to match as closely as possible the average particle refractive index. However, due to the strong optical anisotropy of batch A particles, the need to reduce the refractive index mismatch is not compelling, and the original samples A_1–A_3 were simply diluted in water by a factor of ten. DDLS correlation functions were measured at fixed scattering angle $\vartheta = 15°$. Since at $\lambda = 633$ nm this corresponds to $q = 3.46 \times 10^{-4}$ cm^{-1}, for particles with a radius smaller than 100 nm the ratio of the translational to the rotational contribution to the decay rate $\Gamma_T/\Gamma_R = 2/9(qR)^2$ is less than 3%, and the decay of $g_{VH}(t)$ is essentially due only to rotational diffusion.

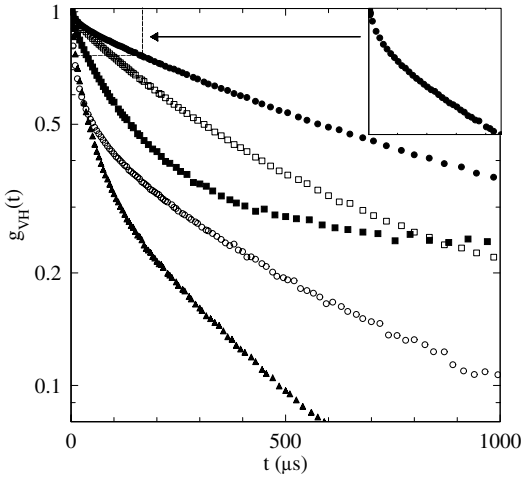

Figure 4. Depolarized field correlation functions for the original sample batch A_0 (○) and for separated fractions A_1 (●), A_2 (□) and A_3 (■), with the short-time behaviour of $g_{VH}(t)$ for sample A_1 expanded in the inset. DDLS results for the upper surnatant phase after three separation steps (▲) are also shown for comparison.

A preliminary estimate of the particle size for the original batch (sample A_0), obtained by a regularized inverse Laplace transform (CONTIN) of polarized DLS correlation functions and shown in the inset of figure 3, suggests a wide distribution, with a broad maximum roughly centred around an effective hydrodynamic radius $R \approx 20$ nm but extending up to much larger sizes. Indeed, the DDLS correlation function for sample A_0 shown in figure 4 displays a markedly non-exponential shape, which can be hardly fitted using a simple cumulant expansion. Conversely, $g_{VH}(t)$ for the first separated phase, which looks approximately exponential over most of its decay range, shows that sample A_1 has a much lower polydispersity. The inset shows that, however, a small number of much smaller particles can still be detected. The DDLS correlation function for sample A_2 shows that the second fraction is composed by particles with a smaller average size, but also that the degree of polydispersity is rather higher. Similarly to what we found for the PFA + FEP mixture, the long-time tail in g_{VH} for sample A_3 suggests that formation of small amounts of large, irreversible aggregates may be associated to phase separation at high surfactant concentration. Finally, the remaining surnatant after separation of fraction A_3, although mainly composed by small particles, still displays the presence of larger objects. We can therefore conclude that the fractionation method looks very promising to separate out relatively monodisperse fractions of large particles, but performs poorly in separating out the smaller components.

3.3. Fractionation of narrow size distributions

It is interesting to inquire about the size resolution of depletion fractionation. Therefore, we have selected to work on a concentrated suspension of small spherical particles obtained by μE polymerization of PFA, having an original solid content of about 30% w/w (batch B). Figure 5 shows that the DLS field correlation function for the original batch (sample B_0) is almost exponential, giving an average particle radius $R = 24$ nm and a polydispersity lower than 10%. Nonetheless, since separation of small sediments was still observed by adding Triton at $c_S > 13.5\%$, the original batch was subjected to a fractionation protocol similar

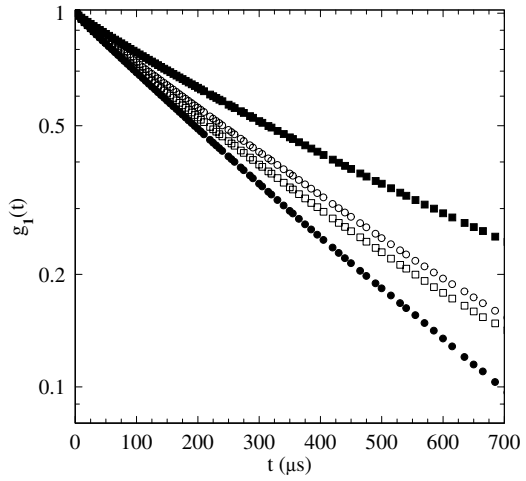

Figure 5. Polarized field correlation functions for samples B_0 (●), B_1 (■), B_2 (○) and B_3 (□).

to that described for sample A. Separated phases were extracted for $c_S = 14.8, 16.6, 18.2\%$ (samples B_1, B_2, B_3 respectively), and amply diluted in water in order to make the effect of Triton on the solvent viscosity negligible. Figure 5 shows that the single fractions are still composed by reasonably monodisperse particles, but with average sizes larger than the original one. The average hydrodynamic radii for the three fractions are found to be $R_1 = 34.5$ nm, $R_2 = 27.5$ nm and $R_3 = 25.5$ nm respectively. By evaluating the amount and density of the sediment, sample B_1 was found to constitute about 5% of the original solid content. Such a small number of particles with a size only 40% larger than the average can hardly be detected by common algorithms aimed to reconstruct particle size distribution from DLS data. Still, large-size 'tails' of the distribution can be filtered out by depletion fractionation.

4. DDLS from optically anisotropic 'fibrillar' particles

4.1. Sample preparation and features

In specific conditions, μE polymerization of PTFE may yield particle size distributions characterized by widely distinct morphologies. The most abundant component is made of spherical particles, with a typical diameter of few tens of nanometres, and of polydisperse short rods with a limited axial ratio, shown for instance in figure 6(A). In addition, however, sediments mainly composed of slender, fibrillar particles (barely visible in figure 6(B)) form over long times at the bottom of the batch container (we notice in passing that electron microscopy characterization of perfluorinated polymer particles is rather hard, since PTFE melts very easily under a TEM electron beam, while SEM generally lacks a sufficient resolution). The method described in section 3 has been used to fractionate a suspension with this composition morphology.

In order to obtain a sufficient amount of concentrated fractions, separation has been accomplished starting from a large batch (about 1 l). Phase segregation was observed for $c_S \gtrsim 5\%$, and the fraction we shall refer to in what follows corresponds to separation with $c_S = 6\%$. The separated fraction was extensively dialysed against distilled water in order to get rid of most of the surfactant. Index matching was then performed by slowly adding glycerol up to a weight fraction of about 35% w/w. For the index-matched suspension, density

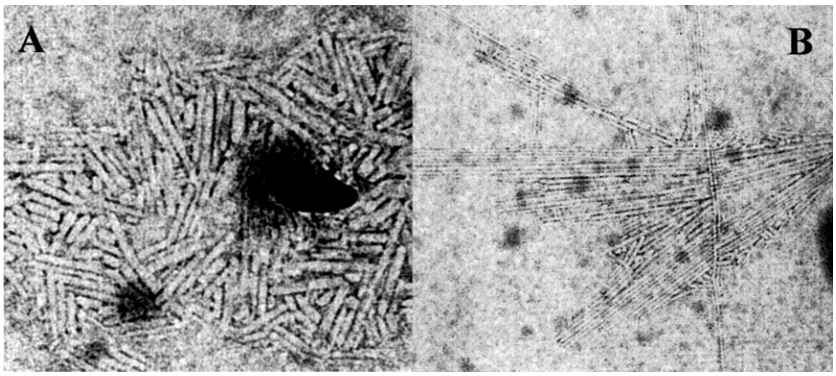

Figure 6. (A) TEM picture of the original suspension used to fractionate batch C. (B) Traces of fibrillar structures present in the latex sediment (courtesy of Ausimont S.p.A.)

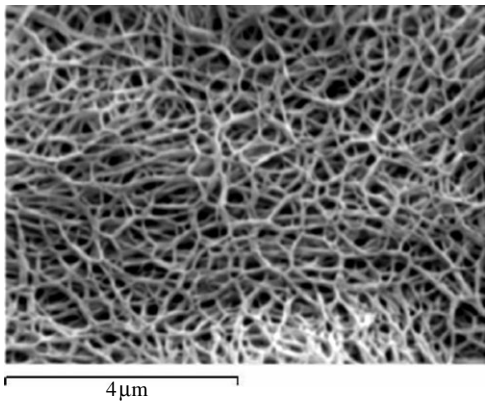

Figure 7. SEM picture of batch C. The original batch has been preliminarily diluted, filtered on a polycarbonate membrane, extensively washed with distilled water and finally coated with an evaporated gold film. The bar length is 4 μm.

measurements yield a particle volume fraction $\Phi_0 \approx 0.02$, which we shall take as nominal concentration for the 'mother' batch (batch C). So far, we have found it rather difficult to obtain reliable electron microscope images of batch C. Very dilute suspensions allowed us to observe single very long, fibrillar structures, which however showed clear hints of partial melting. An overall picture of the sample structure can nonetheless be extracted from the SEM picture of a more concentrated dispersion in figure 7, showing a tangled fibrillar mesh. Although partial fusion of single particles might be possible, the picture suggests a typical straight 'persistence length' in the hundreds of nanometres to micrometre range.

Batch C has very distinctive optical properties. When gently shaken and viewed between crossed polarizers, the sample indeed shows very pronounced shear birefringence, persisting up to tens of minutes (see figure 8, left). However, the birefringence progressively vanishes, and at equilibrium the sample looks fully optically isotropic. Polarization microscopy reveals nonetheless the presence in still samples of strongly birefringent 'tactoids', that is spindle-shaped regions with a typical size in the range of tens of micrometres shown in figure 8, right, which slowly grow with time. Quantitative analysis of the intensity profile shows that tactoids have rotational symmetry along the 'spindle' axis. This texture is normally associated with the

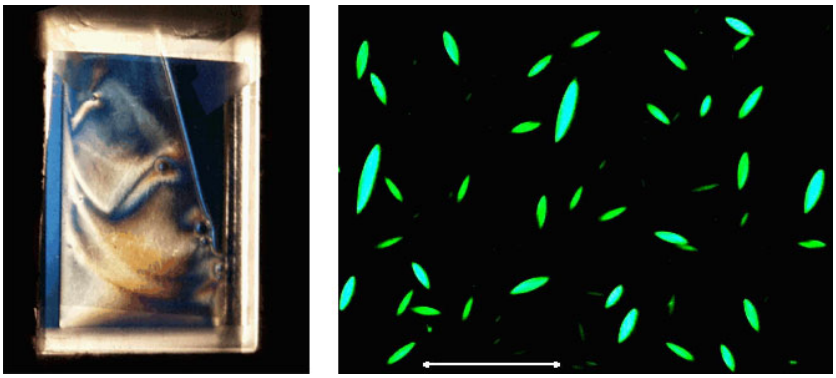

Figure 8. Left: view between crossed polarizers of shear-induced birefringence textures in batch C. Right: polarization microscopy picture of spindle-shaped tactoids. The bar length is 100 μm. (This figure is in colour only in the electronic version)

nucleation and growth of a nematic phase. In colloid science, it has for instance been observed by van Bruggen [11] in beautiful studies of liquid-crystal forming dispersions of boehmite rods. However, no segregation of a macroscopic nematic phase has been observed on a timescale of weeks. Even more, no appreciable sedimentation could be observed by centrifuging the sample at more than 500 g for about 1 h. As we shall see, batch C is indeed very near to being a gel- (or glass-) like phase. The observed morphology rapidly becomes much less evident by diluting batch C, and tactoids essentially disappear for $\Phi \lesssim 0.8\Phi_0$. A full discussion of the sample morphology and phase behaviour is not however the subject of the present study, and is deferred to a future publication. In this preliminary survey we shall mainly concentrate on diffusion properties, and shall particularly discuss the nature of the information that can be extracted from DDLS measurements.

4.2. DDLS from anisotropic particles

Let us briefly recall some basic theoretical aspects of DDLS from dilute and concentrated suspensions of optically anisotropic particles. For dilute suspensions of anisotropic particles with size much smaller than q^{-1}, particle translations and rotations decouple, and the scattered field is simply amplitude modulated by rotations, in addition to the usual phase modulation due to translational diffusion. As we anticipated in section 3, $g_{VH}(q,t)$ turns out to be a simple exponential with an expression for the decay rate Γ_{VH} where a q-independent term, proportional to D_R, adds to the usual translational diffusion contribution, quadratic in the scattered wavevector.

Things are different for concentrated suspensions. For spherical particles interacting via an isotropic potential, rotations of different particles rigorously decouple. As a main consequence, the coefficient of the quadratic term in Γ_{VH} can be shown to be proportional to the concentration-dependent particle *self*-diffusion coefficient D_S, at variance with DLS, which measures *collective* diffusion [8]. Depolarized light scattering has, in other words, close analogies with incoherent neutron scattering from simple liquids. Conversely, it is not known whether or to what extent rotational–translational decoupling pertains in concentrated suspensions of rodlike particles, even if they have a length $L \ll q^{-1}$.

Theory becomes much more complicated, even in the dilute limit and in the Rayleigh–Debye–Gans scattering approximation, for long rodlike particles with $L \gtrsim q^{-1}$, because of two

basic facts. First of all, rotations on the scale of q^{-1} induce a *phase* modulation of the scattered field, which combines with the translational contribution. Moreover, translations and rotations are hydrodynamically coupled in the particle diffusion equation. The theory of single-particle DDLS from long optically anisotropic rods has been developed by Aragón and Pecora, both neglecting hydrodynamic coupling [9] and in the more complex full-coupling case [10]. We shall simply recall the general features of their method and results. The starting point is to regard the particle as composed by small optically anisotropic segments, and then calculate the depolarized scattered field by explicitly evaluating positional and orientational correlation of the different segments dictated by the specific particle geometry. Within the decoupling approximation, the depolarized scattering correlation function for thin rods is given by

$$g_{VH}(q,t) = N \exp(-q^2 D_T t) \sum_{s \geqslant 2, even} (2s+1) C_s^{VH}(x) \mathrm{e}^{-s(s+1)D_R t}, \tag{1}$$

where $x = qL/2$, D_T is the average of the rod translational diffusion coefficients along the principal axes and $C_s^{VH}(x)$ are quadratic forms of particle 'shape factors' defined in terms of spherical Bessel functions. The structure of $g_{VH}(q,t)$ in the presence of coupling, although much more complicated, has an expression similar to equation (1), with the main difference that each relaxation is split into two contributions having slightly different time constants, with weighting coefficients having a very complicated dependence on x and on the roto-translation coupling parameter $\gamma = 3q^2 D_T / D_R$. Evaluation of $g_{VH}(q,t)$ requires therefore an elaborate numerical calculation for each scattering angle. We can however try to extract some general aspects of the solution. Since both the weighting coefficients and the relaxation times depend on q, the initial decay rate of $g_{VH}(q,t)$ is no longer expected to scale linearly with q^2. Coupling is particularly significant at large γ, that is for long rods at large q. However, in the very same conditions D_R is much smaller than $D_T q^2$, and since the decay rates of the single correction terms are proportional to D_R, their overall contribution to G_{VH} may not be too large. For instance, an explicit calculation by Aragón and Pecora for thin rods with $qL \sim 6$ shows that the leading term for g_{VH} is given by $g_{VH} \approx \mathrm{e}^{-D_T q^2 t}[0.85\mathrm{e}^{-5.42 D_R t} + 0.15\mathrm{e}^{-6.25 D_R t}]$, which could not be distinguished at all from $g_{VH} = \mathrm{e}^{-(D_T q^2 + 6D_R)t}$ using common light scattering methods. In the limit of $q = 0$ the decay rate is of course always given by $\Gamma_{VH} = 6D_R$.

Theory becomes even more complicated if the particles are flexible. For Gaussian coils made of anisotropic segments, expressions for the polarizability tensor do exist [14], but we are not aware of any general theory of DDLS from rods with finite rigidity. In the limit of very flexible coils, the concept of a rigid rotational motion obviously loses precise meaning. The coils performs internal motion which can be described as a superposition of modes using for instance the Rouse model [16]. The rotational relaxation time of a polymer coil can actually be *defined* as the longest relaxation time τ_R of the end-to-end vector correlation function $\langle R(0)R(t)\rangle$, which coincides with the slowest Rouse relaxation time. In some sense, τ_R is a 'true' rotational time, since the most probable shape of a Gaussian chain is ellipsoidal, with the longest axis parallel to the end-to-end vector [14]. We also point out that the other relaxation modes contribute only at very short times (the second relaxation time, for instance, is a factor of nine shorter than τ_R).

For concentrated dispersions of long rods, coupling between rotations and translations, and also between rotations of different particles, can only be supposed to become stronger. Because of coupling, depolarized scattering is no longer fully incoherent, and therefore $g_{VH}(q,t)$ ceases to be directly related to self-diffusion (or, more precisely, to be the self-intermediate scattering function). A very open question is therefore whether DDLS essentially measures collective diffusion such as conventional DLS, or rather a 'mixture' of the two diffusion processes. This question can be profitably addressed dealing with suspensions of particles interacting via a repulsive potential, where collective and self-diffusion display opposite trends as a function of

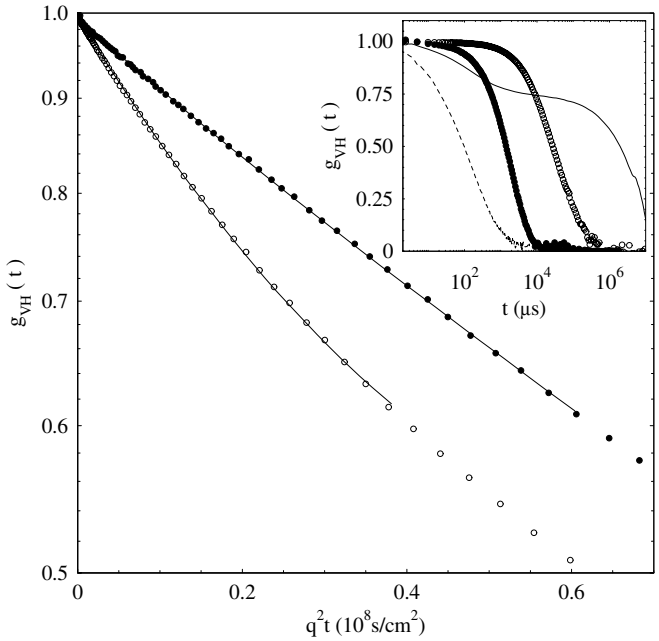

Figure 9. Short-time decay of DDLS correlation functions for batch C at $\vartheta = 130°$ (●) and $\vartheta = 20°$ (○), plotted versus q^2t. Full correlation functions are compared in the inset to $g_{VH}(t)$ obtained at $\vartheta = 20°$ (full curve) and 130° (broken curve) for a dilute sample of the original latex before fractionation.

concentration, the former increasing while the latter decreases with c. It should therefore be easy to settle the problem even using non-fully-ideal systems.

4.3. Single-particle limit

We first discuss DDLS results from a dilute suspension at particle volume fraction $\Phi \approx 0.0013$, obtained by diluting the original batch in glycerol/water at 35% w/w.

The inset of figure 9 shows that the DDLS correlation functions measured at scattering angles of 130° ($q = 2.47 \times 10^5$ cm^{-1}) and 20° ($q = 0.47 \times 10^5$ cm^{-1}) are totally different from $g_{VH}(t)$ obtained at the same angles for the non-fractionated latex diluted in the same glycerol/water solvent. For the original latex, $g_{VH}(t)$ at 20° displays an extremely broad decay, characterized by two main decay rates roughly differing by four order of magnitude. Conversely, $g_{VH}(t)$ at 130° has a much faster decay corresponding to translational diffusion of polydisperse small particles with an average size around 10 nm. This different behaviour is due to the fact that large particles, which have a strongly forward-peaked form factor, do not appreciably contribute to the intensity scattered at large angles. The main body of figure 9, which displays the short-time behaviour of $g_{VH}(t)$ for batch C (plotted for graphical convenience as a function of q^2t), shows that the shape of g_{VH} measured at $\vartheta = 130°$ is very nearly exponential, while larger deviations are present at $\vartheta = 20°$. Fitting the correlation function measured at $\vartheta = 130°$ with a two-cumulant expression $\ln[g_{VH}(q,t)] = -\Gamma t + \Gamma_2 t^2$, we found a polydispersity index corresponding to a size distribution with variance $\sigma^2 = \Gamma_2/2\Gamma^2 \approx 0.2$. This value should be considered as an upper limit, since deviation from a pure exponential shape could be due, as we have previously discussed, to roto-translational

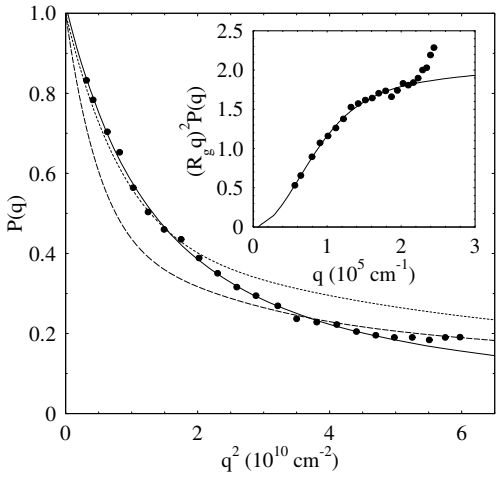

Figure 10. Polarized form factor for a diluted sample of batch C. Full curves are fits to the Debye structure function (equation (3)). Broken curves are rigid-rod form factors for rod length $L = 0.5\ \mu$m (short dashes) and $L = 0.65\ \mu$m (long dashes). The same data are shown as a 'Kratky plot' in the inset.

coupling. The polydispersity index for the correlation function obtained at $\vartheta = 20°$ is about three times larger than at $\vartheta = 130°$. This result is consistent with the fact that the decay rate at large q is essentially determined by D_T, while in the limit of $q = 0$ it is due only to rotational (orientational) correlation. Since, in general, rotational diffusion scales as the inverse of the cube of the particle size L, while D_T only as L^{-1}, the polydispersity for $q \approx 0$ is indeed expected to be about three times larger than at large q.

We have tried to extract information about the particle shape from static light scattering measurements on a sample made by diluting batch C by a factor of 20 in pure water. The obtained polarized form factor cannot be properly fitted with an expression for monodisperse hard rods. Figure 10 shows indeed that the form factor for a slender rod with length $L = 0.5\ \mu$m, which approximately fits the low-q behaviour, completely fails to describe the large-q behaviour, which conversely can roughly be fitted using a rod length $L = 0.65\ \mu$m. Since these values could be within the size standard deviation obtained from D_T, it is possible that a suitable size distribution may give a better fit. However, we may wonder whether the shape of $P(q)$ might rather be due to partial rod flexibility. Therefore, we shall try to borrow from polymer physics a possible 'statistical' description of $P(q)$. The form factor for a *fully* flexible coil is given by the Debye structure function:

$$P(x) = \frac{2}{x^2}[\exp(-x) + x - 1], \tag{2}$$

where $x = (qR_g)^2$ and R_g is the coil gyration radius. Figure 10 shows that, surprisingly, equation (2) gives a much better fit using a gyration radius $R_g \approx 0.15\ \mu$m, which corresponds to an average end-to-end distance $\overline{R} = \sqrt{6}R_g \approx 0.35\ \mu$m. The internal rigidity of a semi-flexible 'wormlike' chain yields deviations from the Debye structure function at high q. In order to give an estimate of particle rigidity, in the inset of figure 10 we plot $(R_g q)^2 P(q)$ versus q. For a fully flexible chain, this 'Kratky plot' should saturate to two for $q \gg R_g$ [15]. The quasi-linear increase which is experimentally found at large q witnesses instead the presence of a rather large rigidity persistence length, which from the plot can be be roughly estimated to be $l_p \approx 50$ nm.

Although we are not in a position to claim that this 'semi-rigid-coil' description corresponds to the real morphology of the particles, we observe that DDLS data are also consistent with the model. The first cumulant Γ_{VH} for $g_{VH}(q,t)$ measured at different angles is plotted in figure 11, together with results for higher volume fractions, to be discussed later. First of all, we observe that Γ_{VH} shows reasonably good scaling with q^2 in the whole investigated q-range, so that, within our experimental accuracy, we do not find strong effects of coupling on $\Gamma_{VH}(q)$. Fitting the data as $\Gamma_{VH} = \tau_R^{-1} + D_T q^2$ we obtain $D_T = (7.4 \pm 0.2) \times 10^{-9}$ cm^2 s^{-1}, $\tau_R = 0.028 \pm 0.006$ s. The translational diffusion coefficient for a flexible coil is related to its gyration radius by [14]

$$D_T \approx 0.2 \frac{k_B T}{\sqrt{6}\eta R_g}, \tag{3}$$

where η is the solvent viscosity. From equation (3) and the experimental value for the solvent viscosity $\eta = 2.508$ cP measured with an Ubbelhode viscosimeter, we obtain $R_g = 0.18 \pm 0.01$ μm. As discussed before, the quantity which better corresponds to a rotational diffusion coefficient for a flexible object is the longest internal relaxation time, which is related to R_g by [14]

$$\tau_R \approx \frac{5.85\eta R_g^3}{k_B T}. \tag{4}$$

From the experimental value for τ_R we obtain $R_g \sim 0.20 \pm 0.02$ μm. Translational and rotational diffusion therefore give values for the gyration radius that are within 20 and 30% respectively of the value derived from $P(q)$. We notice that, had we assumed the particles to be rigid rods, both the rod length L and the length-to-diameter ratio L/b could have been calculated using

$$\begin{aligned} D_T &= \frac{k_B T}{3\pi\eta L} \ln L/b \\ D_R &= \frac{3k_B T}{\pi\eta L^3}[\ln L/b - \delta], \end{aligned} \tag{5}$$

where $\delta = 0.8$ in the simplest approximation [12] and is slightly dependent on L/b in more refined models [13]. Equation (5) yields $L \approx 0.95 \pm 0.08$ μm, which is inconsistent with static data. The axial ratio can be estimated as $L/b \approx 50$. Although this quantity appears logarithmically in equation (2), and therefore is subjected to much larger error, a rod diameter of about 20 nm seems definitely to be much smaller than the average value $d \approx 60$–80 nm that can be guessed from the mesh thickness in figure 7. Finally, as concerns roto-translational coupling, if we assume that the average end-to-end distance plays the role of an 'effective' length L_{eff}, we have $qL_{eff} \approx 9$, which, as previously discussed, is not a very large value. For 1 μm long hard rods, the q-scaled size is $qL \approx 24$, and coupling would surely be more serious.

4.4. Concentration dependence

We turn now to the concentration dependence of $g_{VH}(q,t)$ observed in suspensions prepared by diluting batch C with index-matched solvents. We first point out that, consistently with macroscopic observations of the progressive disappearance of shear-induced textures, all correlation functions are found to be ergodic (that is, fully decaying to zero over sufficiently long delays) up to the original batch concentration. However, approaching Φ_0, intensity fluctuations became extremely slow, and reliable data could be taken up to particle volume fractions $\Phi \approx 0.8\Phi_0$. As further discussed later, we observed moreover that the shape of the

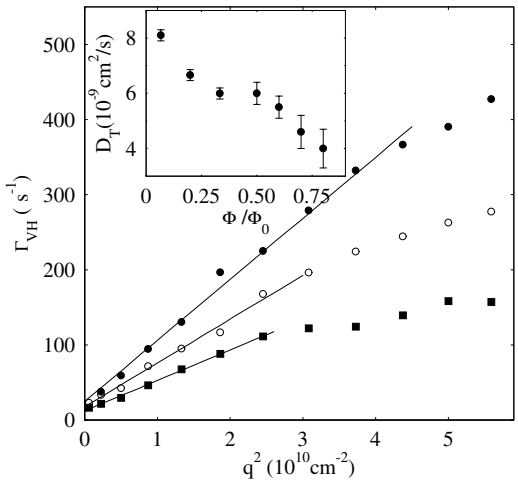

Figure 11. First cumulant of $g_{VH}(q,t)$ for some of the investigated samples at $\Phi/\Phi_0 = 0.07$ (●), 0.33 (○) and 0.8 (■). Linear fits extend up to the maximum q-value used to obtain the short-time diffusion coefficients D_T shown in the inset.

correlation function becomes less and less exponential by increasing Φ. Nonetheless, it is always possible to derive an initial decay rate of $g_{VH}(q,t)$ by fitting the correlation function at sufficiently short times using a two-cumulant expansion.

Figure 11 shows the wavevector dependence of the first cumulant Γ_{VH} obtained for some of the investigated samples. We can notice that deviations of Γ_{VH} from a linear dependence on q^2 become more pronounced by increasing Φ. Flattening of $\Gamma_{VH}(q)$ at large q, which is probably a mark of consistent roto-translational coupling at high concentration, does not allow us to extract a translational diffusion coefficient from a linear fit of the decay rate over the whole q-range. Therefore, as shown in figure 11, a linear fit of $\Gamma_{VH}(q)$ was performed only in a limited q-range. The derived diffusion coefficient D_T, shown in the inset of figure 11, should then be considered as a short-time, low-q limit. The plot shows that D_T decreases with Φ, dropping for $\Phi = 0.8\Phi_0$ to slightly less than half of the dilute-limit value. The large error bars at high Φ are due to the increasingly shorter time range where $g_{VH}(q,t)$ could be properly fitted in order to derive the first cumulant Γ_{VH}. Although the experimental accuracy is much poorer, a decreasing trend with Φ can also noticed for D_R, but a finite short-time rotational diffusion coefficient seems to persist up to $\Phi = 0.8\Phi_0$.

A puzzling feature of the observed behaviour is that D_T monotonically decreases with Φ, as one could predict for a *self*-diffusion coefficient, and contrary to what is expected for collective diffusion of particles (or coils) interacting via a repulsive excluded volume potential, which should conversely *increase* with concentration. This seems to suggest that, even in concentrated dispersions, $g_{VH}(q,t)$ might still essentially behave as a self-intermediate scattering function. In view of the strong coupling between rotational diffusion of distinct particles, this finding is utterly surprising. One may guess that decoupling could still hold, provided that dynamics is probed only for sufficiently short times. However, the following discussion of the full shape of $g_{VH}(q,t)$ shows that the observed trend of translational diffusion with concentration is retained through the whole decay of the correlation function.

Figure 12 shows a few depolarized correlation functions obtained at $\vartheta = 120°$ for some of the investigated samples. While a two-cumulant fit works pretty well for the most dilute solution, $\ln[g_{VH}(q,t)]$ seems to bend continuously in time at larger Φ, witnessing the

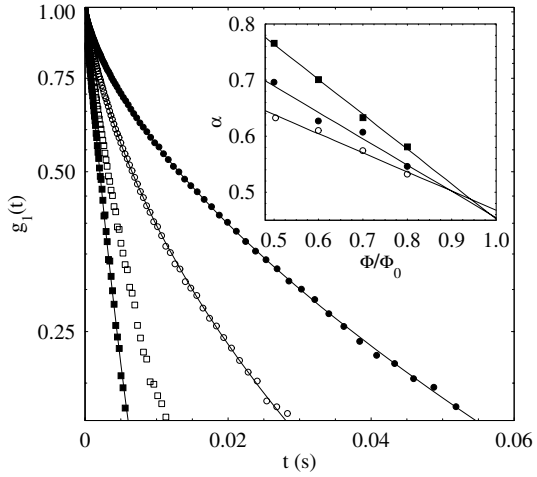

Figure 12. Depolarized correlation functions obtained at $\vartheta = 120°$ for $\Phi/\Phi_0 = 0.1$ (■), 0.25 (□), 0.5 (○) and 0.8 (●). Full curves are stretched-exponential fits of the correlation functions at $\Phi/\Phi_0 = 0.5$ and 0.8, while $g_{VH}(t)$ at the lowest concentration is fitted with a two-cumulant expression. Inset: stretching parameter α as a function of Φ/Φ_0 obtained at $\vartheta = 20°$ (○), $\vartheta = 120°$ (■) and averaged over all angular measurements (●).

occurrence of many relaxation times. Therefore, extracting a meaningful short-time diffusion coefficient from the initial slope of $g_{VH}(t)$ becomes progressively harder at larger Φ. A commonly used trial fit function for broad distributions of relaxation times is a stretched exponential

$$g_{VH}(t) = \exp[-(t/\tau)^{\alpha}], \tag{6}$$

which can be shown to be the exact asymptotic solution for the long-time behaviour of the continuous superposition of many exponential relaxations. The full curves in figure 12 show that the full correlation functions can indeed be fitted quite well using this functional form, except at very short times (corresponding, for instance, for the largest volume fractions to less than a 10% of the total decay of $g_{VH}(t)$), where a finite initial slope can be still defined. The same considerations are valid for all scattering angles when $\Phi/\Phi_0 \gtrsim 0.3$. The inset shows that, for fixed volume fraction, the 'stretching' exponent α slightly depends on q, and approaches for large Φ a value $\alpha \approx 0.5$. For the superposition integral leading to the stretched-exponential shape, this corresponds to an exponentially decreasing distribution of relaxation times [17].

Whatever the shape of the correlation function, we can always define an average decay time as

$$\tau_{avg} \doteq \int_0^{\infty} g_{VH}(t)\,\mathrm{d}t, \tag{7}$$

which for a stretched exponential is related to the decay constant τ by $\tau_{avg} = \alpha^{-1}\Gamma(\alpha^{-1})\tau$ (where $\Gamma(x)$, not to be confused with a decay rate, is the ordinary gamma function).

Figure 13 shows that the average decay rate $\Gamma_{VH}^{avg} = (\tau^{avg})^{-1}$ scales linearly with q^2 and, in contrast to what has been found for the short-time diffusion constant, no 'flattening' at high q seems to be present. The plot also shows that, for $\Phi/\Phi_0 = 1/3$, Γ_{VH}^{avg} calculated from the fit parameter τ closely agrees with the value found from a direct numerical integration of the full correlation function, confirming that the experimental correlation functions can be well described as stretched exponentials. The slope of Γ_{VH}^{avg} versus q^2 yields an 'average'

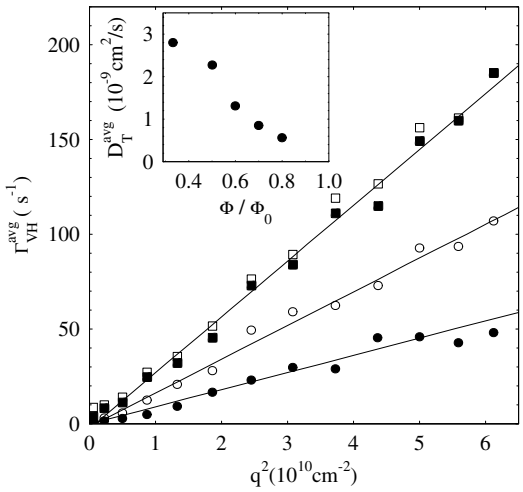

Figure 13. Average decay rate of $g_{VH}(q,t)$, obtained by fitting the correlation functions of some of the investigated samples with a stretching exponential and calculating Γ_{VH}^{avg} as explained in the text. Volume fractions are $\Phi/\Phi_0 = 1/3$ (■), 0.6 (○) and 0.8 (●). For comparison, we also show Γ_{VH}^{avg} calculated for $\Phi/\Phi_0 = 1/3$ by numerical time-integration of $g_{VH}(q,t)$ (□). The inset shows D_T^{avg} derived from linear fits to the data.

translation diffusion coefficient D_T^{avg}, which is shown in the inset. Compared with the short-time value D_T, D_T^{avg} shows a more pronounced, almost linear decrease with Φ, and becomes vanishingly small for values of Φ very close to Φ_0. As concerns the zero-q extrapolation of Γ_{VH}^{avg}, which would give a value D_R^{avg} for the average rotational diffusion coefficient, it is hardly distinguishable from zero for $\Phi \gtrsim 0.5\Phi_0$. It is therefore possible that rotational motion in such concentrated suspensions is non-ergodic, and limited to finite angular fluctuations. Conversely, although the intercepts of the linear fits to the data present some incertitude due to data scattering, correlation functions taken at $\vartheta = 15°$, with long accumulation time and pretty good statistics, seem definitely to imply free rotation at least for $\Phi \lesssim 0.3\Phi_0$. One may wonder whether the fact that D_T^{avg} vanishes around Φ_0 (which is, after all, nothing but the concentration of the original sample batch!) is simply incidental. We recall however that the original sample batch withstood further concentration, not only by gravitational settling but also by centrifuging (this is actually the only reason why Φ_0 is the largest volume fraction we have been able to investigate). Vanishing of D_T^{avg} might be therefore due to the onset of a macroscopic 'glassy' behaviour, anticipating and hindering full separation of a nematic phase.

5. Conclusions

We have shown that depletion effects induced by nonionic surfactant micelles can be profitably exploited in order to perform *a posteriori* fractionation of polydisperse fluorinated particle lattices. In particular, the developed protocol seems to work reasonably well in selecting the largest-size components of a dispersion. By applying the method to specific PTFE lattices obtained by μ-E polymerization, suspensions of 'pauci-disperse' fibrillar particles can be fractionated. We have presented a preliminary investigation of this system, which shows very interesting morphological features and, due to the intrinsic optical anisotropy of the particles, opens to the possibility of studying dynamic depolarized light scattering in suspensions showing mesogenic phases. The observed features of DDLS are quite puzzling.

Although particle size and geometrical anisotropy are rather large, and coupling of rotations and translations at different particles should be expected in the investigated concentration range, the diffusion coefficients that can be extracted both from the short-time and from the full decay of $g_{VH}(q, t)$ decrease with concentration, retaining features which are typical of self-diffusion. This apparent contradiction could probably be settled by developing a more extended theory of DDLS from concentrated suspensions. The fractionation method we have discussed could probably be improved by using different, more efficient, depleting agents, and with some effort dispersion with narrower size distributions can probably be obtained. The opportunity of fractionating long optically anisotropic particles with a narrow size distribution, resembling giant semi-flexible polymers, is particularly alluring, and will allow us to apply DDLS to morphologically and structurally complex colloidal suspensions.

Acknowledgments

We thank very much Ausimont S.p.A., and in particular T Poggio and V Kapeliouchko for the synthesis of the original particle batches, and M Visca for useful discussions and suggestions.

References

[1] Lekkerkerker H N W, Poon W C K, Pusey P N, Stroobants A N and Warren P B 1992 *Europhys. Lett.* **20** 559
[2] See, for instance,
Odijk T 1998 *Biophys. Chem.* **73** 23
[3] See, for instance,
Dijkstra M, Brader J M and Evans R M L 1999 *J. Phys.: Condens. Matter* **11** 10 079
[4] See, for instance,
Evans R M L and Poon W C K 1997 *Phys. Rev.* E **56** 1918
[5] Bibette J, Roux D and Pouligny B 1992 *J. Physique* II **2** 401
[6] Piazza R and Di Pietro G 1994 *Europhys. Lett.* **28** 445
[7] Degiorgio V, Piazza R and Di Pietro G 1996 *Prog. Colloid Polym. Sci.* **100** 201
[8] Degiorgio V, Piazza R, Bellini T and Visca M 1994 *Adv. Colloid Interface Sci.* **48** 61
[9] Aragón S R and Pecora R 1977 *J. Chem. Phys.* **66** 2506
[10] Aragón S R and Pecora R 1985 *J. Chem. Phys.* **82** 5346
[11] van Bruggen M 1998 Liquid crystal formation and diffusion in dispersions of colloidal rods *PhD Thesis* University of Utrecht
[12] Burgers J M 1938 *Verh. K. Ned. Akad. Wet.* **16** 113
[13] Broersma S J 1960 *J. Chem. Phys.* **32** 1626
[14] Doi M and Edwards S F 1996 *The Theory of Polymer Dynamics* (Oxford: Clarendon)
[15] Strobl G 1998 *The Physics of Polymers* (Berlin: Springer)
[16] Rouse P E 1953 *J. Chem. Phys.* **21** 1272
[17] Degiorgio V, Piazza R, Mantegazza F and Bellini T 1990 *J. Phys.: Condens. Matter* **2** SA69